VILNIAUS UNIVERSITY
FACULTY OF PHYSICS
INSTITUTE OF THEORETICAL PHYSICS AND ASTRONOMY

Gediminas Maskeliūnas

INVESTIGATING FOSSIL GALACTIC OUTFLOWS

Master's thesis

Theoretical Physics and Astrophysics

Student	Gediminas Maskeliūnas
Defence permitted	2023-05-25
Supervisor	dr. Kastytis Zubovas
Reviewer:	dr. Jonas Klevas
Head of department	prof. dr. Egidijus Anisimovas

Vilnius 2023

Table of Contents

Introduction 2
1 Central supermassive black hole feedback on galaxy 3
1.1 Formation of outflows 3
1.2 Fossil outflows 4
2 Methodology 6
2.1 Simulation setup 6
2.2 Initial conditions 6
2.3 AGN luminosity 7
2.4 Gas fragmentation 9
3 Results 11
3.1 Morphological evolution and kinematics 11
3.2 Differences in Outflows between Galaxies with AGN and Galaxies with Recently Quiescent AGN 14
3.3 Outflow thermodynamical phases 18
3.4 Outflowing mass 20
4 Discussion 22
Conclusion 24
References 25
Summary 28
Appendix 29

Introduction

Supermassive black hole in its host galaxy center is an important element to the evolution of that galaxy. Discovered relations between supermassive black hole (SMBH) mass and velocity dispersion of their host bulge (Ferrarese & Merritt, 2000) raised a problem: what kind of mechanisms are able to maintain such tight correlations? Active galactic nuclei (AGN) are bright and energetic sources of radiation, and can be found in central parts of the galaxy - galactic bulges. Accreting mass on SMBH feeds it and at the same creates powerful radiation source - acretion disk. Accretion disk is what drives the wind in the AGN, then AGN winds push away surrounding gas and create outflows, a feedback mechanism, which regulate the amount of gas and fragmentation in the galactic bulge. Outflows can take form of elongated conical-structure gas, that are capable moving with radial speeds > 1000 km s^{-1}. Cicone et al. (2014) also show that parameters of outflows correlate with AGN luminosity.

Outflows were found, whose parameters (such as mass flow rates) did not correlate with AGN luminosity and were named fossil outflows (Fluetsch et al., 2019). Analytical predictions (King et al., 2011) show that outflows may remain a significant amount of time, compared to the AGN activity duration. Realistic AGN episodes last from 10 kyr up to several 100 kyr (Schawinski et al., 2015). In this work I run hydrodynamical simulations, with multiple random-uniformly generated AGN luminosity histories, based on the mentioned realistic AGN episode range. I then compare them to less realistic ones where AGN episode is continuous for a 1 Myr.

Aim

The aim of this thesis is to investigate the evolution of large-scale outflows in galaxies with multiple AGN episodes.

Objectives

1. Determine the morphological, kinematical, dynamical and energetic evolution of outflows driven by multiple AGN episodes and determine their phase structure.

2. Determine the salient differences between outflows in currently-active galaxies and galaxies where the AGN episode ended recently.

3. Determine the effect that the episodic nature of AGN has on the propagation of galactic outflows as compared to continuous energy injection.

1 Central supermassive black hole feedback on galaxy

This chapter is based on a Masters coursework Maskeliūnas (2022).

The vast majority of galaxies contain supermassive black holes in the bulge (Kormendy & Ho, 2013), and important relations such as (Ferrarese & Merritt, 2000; McConnell & Ma, 2013)

$$\log\left(\frac{\sigma}{200\mathrm{kms}^{-1}}\right) = \frac{\log\left(\frac{M_{\mathrm{BH}}}{\mathrm{M}_{\odot}}\right) - 8.32}{5.64}; \tag{1}$$

or $M_{\mathrm{SMBH}} \propto M_{\mathrm{bulge}}^{\beta}$, where $\beta = 1.12 \pm 0.06$ (Häring & Rix, 2004; Kormendy & Ho, 2013) were found, the SMBH mass is denoted M_{SMBH}, σ is central velocity dispersion and M_{bulge} is bulge mass. These tight correlations show galaxy and SMBH coevoliution. One of coevolution models suggest, that when SMBH gets fed enough gas, active galactic nucleus (AGN) triggers, which heats up the gas inside the bulge. AGN can work as a feedback mechanism, that consists of SMBH, accretion disk that feeds the black hole and clumpy gas and dust torus around the SMBH. This mechanism can be a direct consequence of merging galaxies (Springel et al., 2005) or secular processes (Smethurst et al., 2019). In the event of mergers, cold gas are pushed towards the centers of galaxies, due to tidal forces, and SMBH is being fed through accretion. The intense radiation that is emitted by an accretion disk manifests in powerful winds, that shock the surrounding gas and thus create large-scale gas outflows. However, in case of secular processes, local inflows from galactic disk to SMBH trigger AGN, resulting in internal outflow feedback on the galaxy rather than the intergalactic medium. Outflows, that move through the central bulge of the host galaxy, can regulate the amount of gas that is in the galaxy. That is important, since the star formation and black hole accretion gravely depend on the amount of cold dense gas, that is available in the ISM. Also, observational data indicate, that parameters, which let us identify outflows such as mass flow rates, correlate with host galaxy luminosity (Cicone et al., 2014)

1.1 Formation of outflows

Typically, outflows are a contributing factor to the $M_{\mathrm{SMBH}} - \sigma$ relation. For such phenomena to occur, a feedback mechanism is necessary during the AGN episode. Dense gas, that fall to the black hole, form an accretion disk, that feeds the SMBH. Subsequently, hot plasma that is in accretion disk, generates intense radiation, that affects the surrounding gas by shocking it with powerful winds, thus creating outflows, which also affect the interstellar medium (ISM) (Zubovas & King, 2019). Authors also show that, the typical wind kinetic energy flow rate is:

$$\dot{E}_{\mathrm{w}} = \frac{1}{2}\dot{M}_{\mathrm{w}} v_{\mathrm{w}}^2 = 0.05\frac{\tau^2 \eta_{0.1}}{\dot{m}} L_{\mathrm{AGN}} \tag{2}$$

where $\dot{m} = \dot{M}_{\rm w}/\dot{M}_{\rm BH}$ is the ratio of wind mass flow rate and BH accretion rate, $v_{\rm w}$ - wind speed, $\eta \sim 0.1$ - accretion disk radiation efficiency and $\tau \simeq 1$ is optical depth.

The AGN generated wind energy in theory it can transfer $\sim 5\%$ of luminosity. Typically, such winds, that travel at relativistic speeds, encounter interstellar medium, then shocks it at hypersonic speeds. Afterwards, outflows can be separated into two kinds: momentum-driven or energy-driven. Such outflows emerge, when AGN wind shocks the ISM. If the shocked wind gas cools faster compared to the timescale of motion of the shock pattern, the momentum-driven flow occurs. However, if the shocked wind gas cools inefficiently, the flow will adiabatically expand into a bubble. The later case will be an energy-driven outflow. It is worth mentioning, that energy-driven flows are much more energetic that momentum-driven outflows (Zubovas & King, 2012). Another important aspect, that affects the outflows is the ISM structure itself. Hot gas, that adiabatically expands into bubble, travels through the ISM and can encounter dense gas clumps, such ass molecular gas clouds. In that case, the outflowing gas might escape through less dense channels allowing for the dense molecular clouds to fall into the SMBH and feed it (Zubovas & King, 2019). It is also important, that AGN episodes last up to several hundred thousand years and typically clustered in time (up to 10^7 yr.) (Hopkins et al., 2005; Zubovas et al., 2022). Outflows can also persist for a significant amount of time (more than 10^6 years) compared to the AGN episode duration. Clusterization in time is defined by a parameter called duty cycle $\delta_{\rm duty}$, it is the ratio of total SMBH activity time and total time, that includes both activity and inactivity periods between the active episodes. Values of $\delta_{\rm duty}$ vary depending on the galaxy, for galaxies with radio-mode feedback $\delta_{\rm duty} \gtrsim 0.69$ (Bîrzan et al., 2012).

1.2 Fossil outflows

While it would seem that outflow parameters such as mass, momentum, and energy flow rates correlate well with AGN luminosity (Cicone et al., 2014), i.e. the activity of the AGN, this is not always the case. Observations of the Marasco et al. (2020) have shown that there are galaxies for which the observed flow properties do not correlate with the analytically determined ideal theoretical prediction. (Stuber et al., 2021) show that, from 90 observed galaxies around 20% had outflows, and only half of these galaxies had an AGN. Such outflows, which do not show a tight correlation with AGN luminosity L are called fossil outflows. Furthermore, observational data support such phenomena, where 4 out of 45 observed galaxies contained fossil outflows (Fluetsch et al., 2019). Authors also mention, that the low fraction of galaxies with fossil outflows is due to the biased sample of analysed galaxies with strong AGN. These four galaxies were characterized by having outflows with very high momentum rate. It was too high, even when assuming that AGNs were transmitting their energy to surrounding gases with 100% efficiency or in other words 100% coupling rate. This led to a conclusion, that such energetic outflows were most likely fossil. Therefore, when AGN activity is decreased, energetic flows can still be observed. King et al. (2011) and Ishibashi & Fabian (2018) theoretical models predict fossil outflow existence. In these models energy ratio $\varepsilon = \dot{E}/L$ values can

be equal to 1% and more (provided radiation trapping occurs due to high dust to gas ratio), where $\dot{E}$ are outflows' energy flow rate. This reveals in more detail which parameters can provide a good description of fossil outflows, which in turn allow us to narrow down the duration of the (former) AGN episode under study and to draw some boundaries. It also might be used as a tool to reconstruct: what was the AGN luminosity during an episode of activity, what was the duration of the previous AGN episode, what might have been the starting AGN luminosity etc. Using a neural network trained on 1D simulated outflows, Zubovas et al. (2022) have shown that they can trace the history of AGN episodes in 46 real galaxies, determine outflow features, and estimate the AGN activity duty cycle, episode duration, bulge gas fraction, and outflow opening angle. It is important to note that typically AGN episodes on average last around $(1-1.5)\times10^5$ yr. Analytical expectations predict that fossil outflows may be detectable up to 10 times longer that the AGN episode itself (King et al., 2011). This gives constraints to the fossil outflows longevity.

2 Methodology

2.1 Simulation setup

In this work, I use Gadget 3 to perform hydrodynamical simulations (Springel, 2005). This code uses smoothed particle hydrodynamics (SPH) numerical method, which for simulation of fluid or solid body mechanics in continuum media. Every SPH particle inside this media interacts with surrounding particles through a defined kernel function W. The main characteristic of this function is smoothing length - h. The value of h determines the size of the smoothing region around each particle. Using an interpolation equation (Dalrymple, 2007)

$$u(s,t) \approx \sum_j \frac{m_j}{\rho_j} W(s - x_j, h) u_j(t) \tag{3}$$

it is possible to interpolate the value of u at $x = s$ coordinate, where m_j is particles' mass, ρ_j is the density in the vicinity of the particle. SPH method is good for astrophysical numerical simulations (Price & Federrath, 2010), because it allows for good conservation of mass, momentum and energy. In this work, simulations are calculated using an SPHS variant (Read & Hayfield, 2012) and Wendland kernel is used (Wendland, 1995; Dehnen & Aly, 2012). The SPHS modification allows the mixing of regions with different densities to be reproduced. The normal SPH code does not allow this. In this work hydrodynamical adaptive smoothing lengths of h_i, for i-th particle are used:

$$\frac{4\pi}{3} h_i^3 \rho_i = N_{\mathrm{ngb}} m_{\mathrm{SPH}}, \tag{4}$$

where $N_{\mathrm{ngb}} = 100$ is the SPH neighbour number, $m_{SPH} = 3700\ \mathrm{M}_\odot$ is the SPH particle mass and ρ_{i} is the i-th particle density. The simulations begin by representing the central galactic bulge with a symmetrical gas shell that is spherical in shape. A turbulent velocity field is then applied which is based on (Dubinski et al., 1995) and (Hobbs et al., 2005). The turbulence is not driven throughout the simulation. A SMBH is placed as a point object in the center of each simulation, and after 1 Myr the AGN activity begins. The whole simulation lasts 5 Myr.

2.2 Initial conditions

In total, 14 simulations are run, divided into two groups distinguished by different velocity fields applied to each simulation. That way it is possible to investigate stochastic differences in particle positions and velocities in the simulation results. The σ parameter characterizes the velocity dispersion of the turbulent gas. And it is the same throughout all the models $v_{turb} \simeq 176\ \mathrm{km\ s^{-1}}$. This parameters' value is derived from the $M - \sigma$ relation (see Eq. 1). For these simulations a typical mass of $M_{\mathrm{bh}} = 10^8\ \mathrm{M}_\odot$ is chosen. From this, it is possible to calculate the bulge mass (McConnell & Ma,

2013):

$$\log\left(\frac{M_{\mathrm{tot,b}}}{10^{11}\ \mathrm{M}_{\odot}}\right) = \frac{\log\left(\frac{M_{\mathrm{BH}}}{\mathrm{M}_{\odot}}\right) - 8.46}{1.05}; \tag{5}$$

which is $M_{\mathrm{tot,b}} = 3.7 \times 10^{10}\ \mathrm{M}_{\odot}$. The gas mass fraction of the bulge is set to 10% for a gas rich galaxy (Guo et al., 2017), therefore I set $M_{\mathrm{gas}} = 3.7 \times 10^{9}\ \mathrm{M}_{\odot}$. Having these parameters it is possible to find the radius for the bulge:

$$R_{\mathrm{out}} = \frac{GM_{\mathrm{tot,b}}}{2\sigma^2}; \tag{6}$$

where σ is bulge velocity dispersion. I then set the boundaries from $R_{\mathrm{in}} = 0.1$ to $R_{\mathrm{out}} = 2.57$ kpc

2.3 AGN luminosity

For these simulations 5 different AGN luminosity histories are generated. Each AGN luminosity history is based on an existing approach of uniformly sampling AGN episodes (Zubovas et al., 2022):

$$4 < \log(t/\mathrm{yr}) < 5.5 \tag{7}$$

where t is randomly uniformly generated length of a single AGN burst. These typically last from ten thousand to a couple of hundred thousand years (Schawinski et al., 2015). In the same manner, the pauses between the AGN episodes are generated, to reach the desired duty cycle of $\delta_{\mathrm{duty}} = 0.5$. Where duty cycle can be defined as:

$$\delta_{\mathrm{duty}} = \frac{t_{\mathrm{episodes}}}{t_{\mathrm{activity}}} \tag{8}$$

where in this case the sum of all AGN episodes is $t_{\mathrm{episodes}} = 1$ Myr, and the activity distribution length, that also includes pauses between episodes is $t_{\mathrm{activity}} = 2$ Myr, spanning from 1 to 3 Myr in the simulation. Figure 1 shows one of the generated AGN history, that is implemented in two simulations. The visualisation depicts square wave like pattern, which shows the frequent AGN bursts and pauses in between.

Table 1. Naming of simulations

A	B
R1A	R1B
R2A	R2B
R3A	R3B
R4A	R4B
R5A	R5B
CA	CB
control-A	control-B

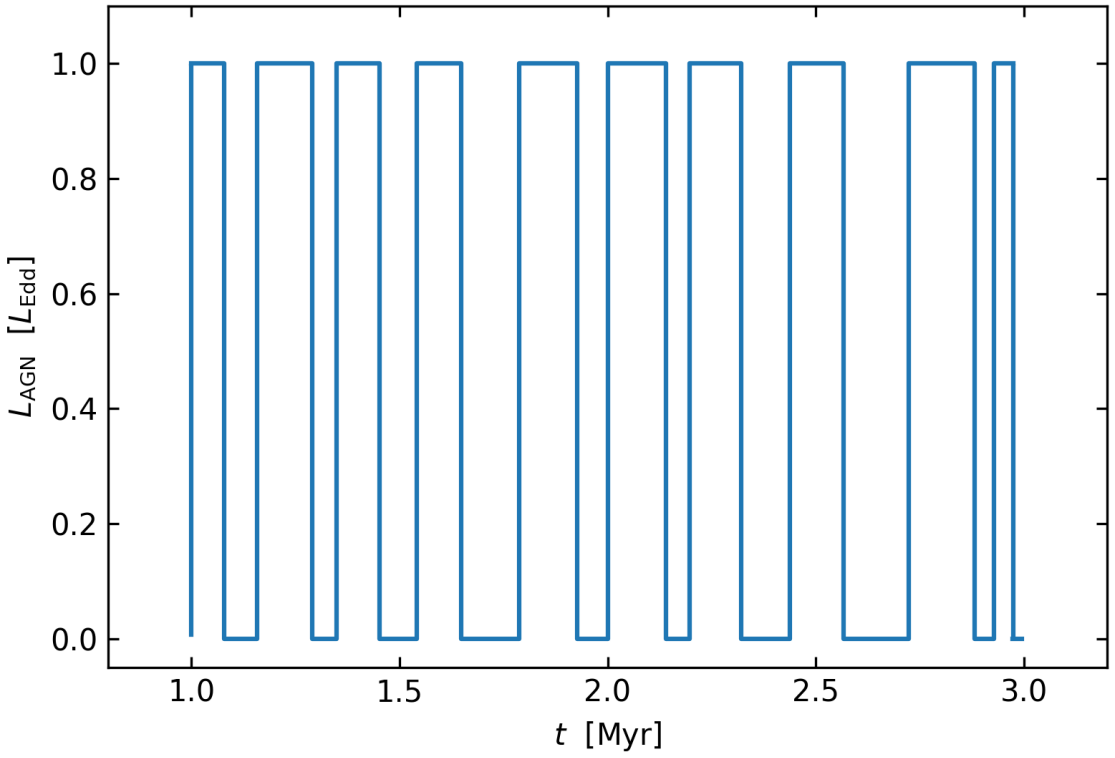

Figure 1. An example of one of AGN luminosity histories. Blue line, square wave like pattern shows AGN activity over 2 Myr. The total activity time is 1 Myr, thus achieving the duty cycle of $\delta_{\rm duty} = 0.5$.

These pseudo-random uniform AGN history distributions are seeded in order to replicate the same AGN activity while applying a different velocity field. In total there are 5 different seeds and each simulation is named from run 1 to run 5 (denoted by an R, following a number) respectively, as seen in the Table 1 as they are separated by two velocity fields, which are named A and B. I also run 2 continuous (denoted by a letter C) AGN activity simulations, with a single episode, lasting from 1 Myr to 2 Myr, to better compare and evaluate the effects of multiple AGN episodes, while injecting the same amount of energy into the simulation. Also, for comparison, control simulations with no AGN activity are calculated. In all simulations, SPH particle count is $N \simeq 10^6$ and during the first

Table 2. Initial conditions

Initial conditions	Values
$M_{\rm BH}, \mathrm{M}_\odot$	10^8
$L_{\rm AGN}/L_{\rm Edd}$	1.0
$R_{\rm in}$, kpc	0.1
$R_{\rm out}$, kpc	2.57
$v_{\rm turb}$, km/s	176
$m_{SPH}, \mathrm{M}_\odot$	3700
$M_{\rm gas}, \mathrm{M}_\odot$	3.7×10^9

million years of evolution all particles that come closer than 0.1 kpc are eliminated. This allows for the 1st AGN episode not to be fully suppressed by a vast amount of gas in the center, and for outflows to form.

For the AGN wind feedback a spherical *windgrid* method is used (Tartėnas & Zubovas, In preparation). The propagation of wind is set to a constant speed $v_{\rm w} = 0.1c$. When particles come into contact with the wind, they receive a proportional share of its energy and momentum, corresponding to their contribution to the density field in the relevant part of the grid. The grid structure used in these simulations is the simplified version of *SREAG* grid (Malkin, 2019). The grid radius is about the same size as the $R_{\rm out}$, which is $r_{\rm grid} = 2.5$ kpc. The radial resolution is

$$\Delta r_{\rm rad} = \frac{r_{\rm grid}}{n_{\rm r}} = 12.5\mathrm{pc} \tag{9}$$

where $n_{\rm r} = 200$ is the amount of layers in the grid. The effective angular resolution is:

$$\Delta r_{\rm Eff.ang.} = \frac{4\pi}{N_{\rm shell}} = 0.0024 \tag{10}$$

where $N_{\rm shell} = 5216$ is the amount of cells in the shell.

2.4 Gas fragmentation

In these simulations, heating and cooling functions for the AGN-affected gas are used. For gas with temperature higher than 10^4 K Sazonov et al. (2005) function is employed. It allows for heating and cooling optically thin gas that is affected by AGN radiation. For gas with temperatures lower that 10^4 K, the Mashchenko et al. (2008) function is used. Furthermore, star formation is possible in these simulations. Having it is necessary to ensure that the simulations do not slow down excessively when dense gas clumps form. To avoid spurious fragmentation, density-dependent temperature floor is implemented, so that gas of ρ cannot reach lower temperature than:

$$T_{\rm floor} \simeq 350 \left(\frac{\rho}{10^{-22} \mathrm{g\ cm^{-3}}} \right)^{\frac{1}{3}} \left(\frac{\mu}{0.63} \right) \left(\frac{m_{\rm sph}}{1600\ \mathrm{M}_\odot} \right)^{\frac{2}{3}} K \tag{11}$$

where μ is mean molecular weight. This equation guarantees that Jeans mass is always resolved for $N_{\rm ngb}$ particles. Furthermore, SPH particles, that reach this temperature floor, are stochastically converted into star particles with a probability of $P = 1 - \exp[-0.1\Delta\, t/\tau_{\rm ff}]$, where $\Delta\, t$ is particles' time-step and $\tau_{\rm ff}$ is the local free-fall time. The star formation efficiency is 0.1 (Dobbs & Pringle, 2013).

3 Results

3.1 Morphological evolution and kinematics

In this section I present the qualitative evolution of the simulations. In Figure 2, two density maps are shown, which are projection in the XZ plane. These maps show gas, which belong to -70 pc < y < 70 pc, therefore we can better see the inner structure of the simulation and certain properties of it. On the left, the first snapshot of every simulation at $t = 0$ Myr is shown, as well as on the right - snapshot at $t = 1$ Myr is shown. Gas have a 1 Myr relaxation period, throughout gas with initial velocities form a turbulent, uneven medium with both dense/clumpy and diffuse areas. We can also see fillament-like structures, which are rather prevalent in all simulations.

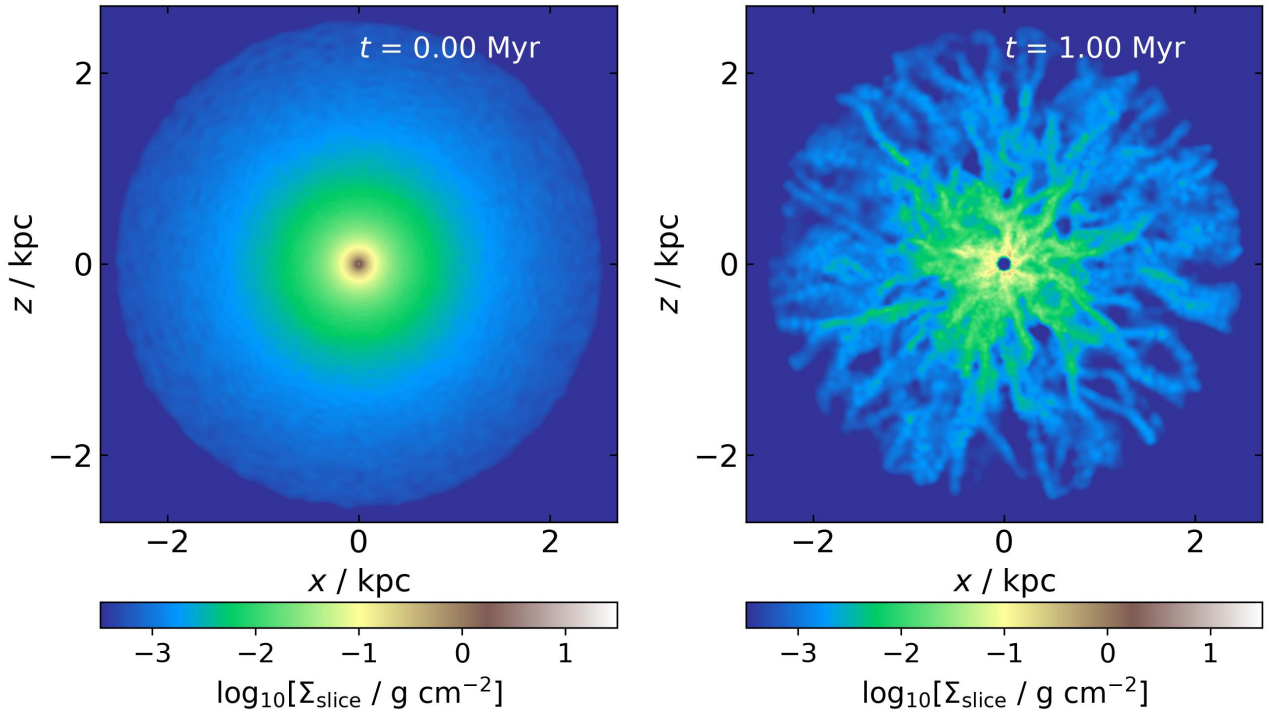

Figure 2. Density evolution of A group simulations. *Left* is density slice at $t = 0$ Myr. *Right* is density slice at $t = 1$ Myr before AGN becomes active.

Next, I analyse a R4A density maps, which are seen in Figure 3. Here, a more zoomed in view is presented. On the left panel at $t = 1.5$ (AGN is inactive), we see some outflows going to positive X and both Y directions, the largest one being on the positive X side. Outflows may take many different forms, but in this case it looks conical-shaped. In general, for outflows it is more easy to expand and flow through more diffuse areas of the ISM, that is also the case in these simulations. Later, during one of the AGN activity episodes (middle pannel) we can see the same outflow (going to positive X direction), which has increased in size. Now it has taken more of a bubble form. In the same map we can see an additional outflow going to negative X direction. In the last panel, which is at $t = 2.5$ Myr, during at the inactive AGN phase, we can see a different view - the evolution has progressed

significantly, and now the outflows seem rather less expressed. That is also due to infalling dense gas, that suppress the outflows.

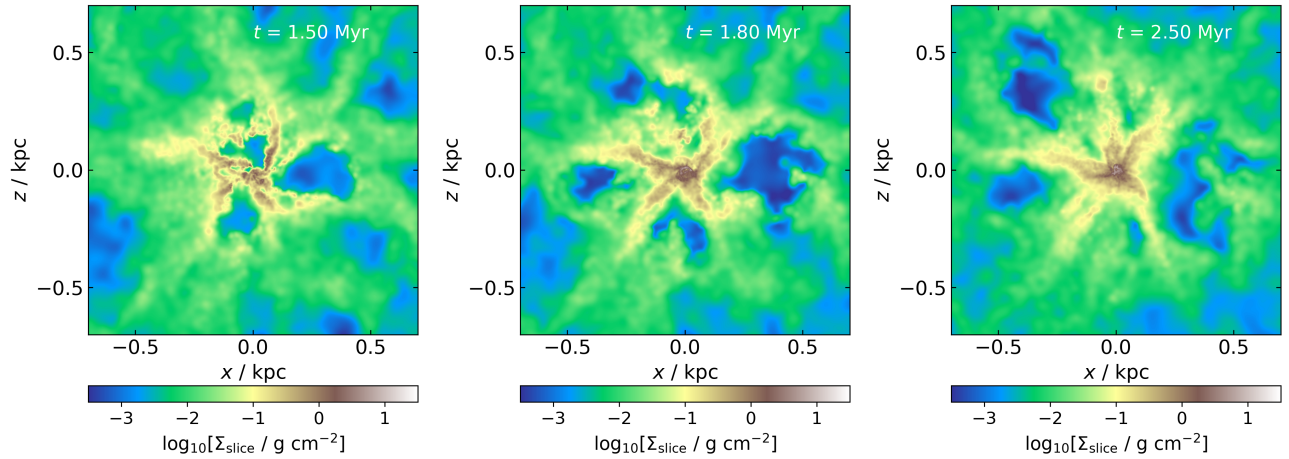

Figure 3. Density evolution of R4A simulation. *Left* is density slice at $t = 1.5$ Myr. *Middle* is density slice at $t = 1.8$ Myr. *Right* is density slice at $t = 2.5$ Myr.

Figure 4 shows 3 velocity maps of the same simulation, with the same timestamps. They show somewhat different view of the outflows. At $t = 1.5$ Myr it is possible to see, the unseen in previous density map, fourth outflow going to negative X direction. These outflows, if looked from this perspective, show a cross-like pattern. The most prominent outflow is the positive X outflow, which now seems more conical/bubble-like, rather than taking a straightforward cone shape. We can deduce its form more accurately from velocity maps, than from density ones. For this outflow velocities reach $v_{\rm rad} > 300$ km s^{-1}. Other outflows flow slightly slower $v_{\rm rad} \sim 100$ km s^{-1}. These outflows can be considered fossil ones, since the AGN at this particular time is inactive. After 300 kyr (middle panel), we can see, that outflows have propagated further from the center, up to 0.6 kpc for the positive Y outflow. However, there is some activity seen in the center, where more red color appears to be concentrated. This is because AGN is active at this particular time, and is inflating the top side outflow. On the right, we see some stationary gas (white patches), which were a part of more massive outflow, that was seen in previous snapshots going to positive X, as well as from smaller outflows, that went to positive and negative Y directions. We can see that one more bigger outflow is still receding away in the upper left corner of the map.

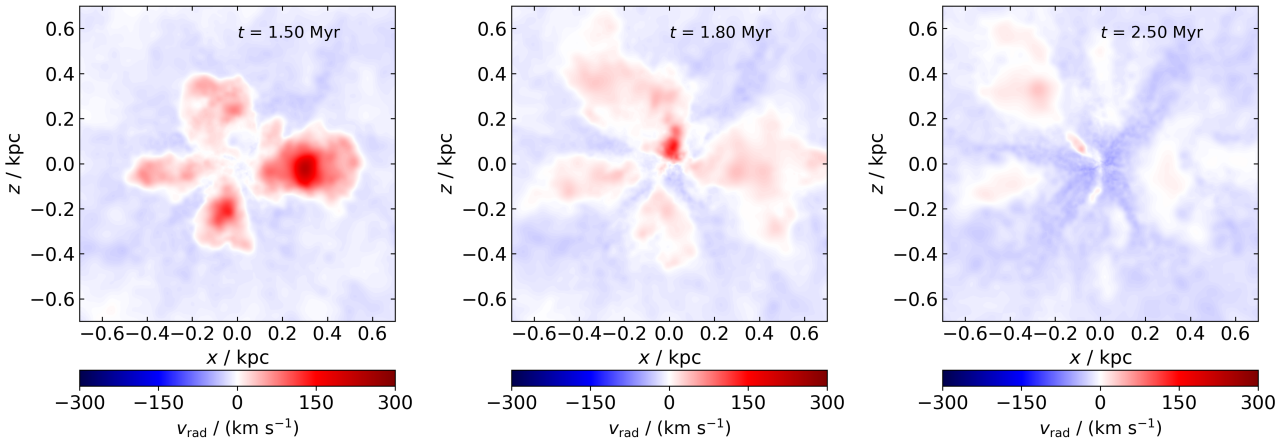

Figure 4. Radial velocity evolution of R4A simulation. Maps show snapshots at $t = 1.5, 1.8$, and 2.5 Myr.

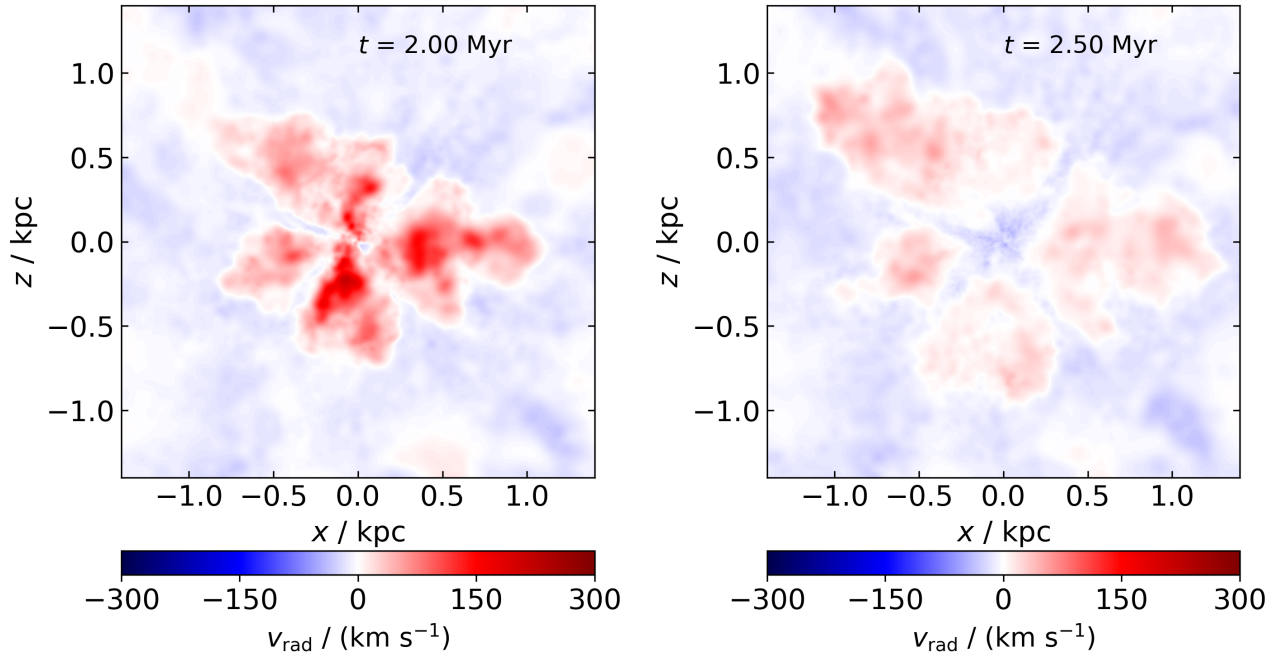

Figure 5. Radial velocity evolution of CA simulation. *Left* is density slice at $t = 2$ Myr. *Right* is density slice at $t = 2.5$ Myr.

In Figure 5 the CA simulation radial velocity maps are shown. Since the AGN episode activity inflates outflows continuously for a million years, they are larger (note the bigger scale of the map) and overall faster in more directions than in previous R4A simulation, reaching $v_{\rm rad} > 300$ km s^{-1} (left panel). They form the cross-like pattern (this is due to both: the projection I choose to view these maps in and stochastic velocity field), expanding to all directions, while maintaining the cone-like shapes. The smallest one being the one that is receding in the negative X direction, and the 2 biggest progressing towards positive X, and positive Y, negative X directions. Though, it is not really clear whether the one, that is receding to negative X direction is small due to to the shortage

of diffuse gas for the outflows to expand through near the AGN, or is it just because the projection is only filtering a side slice of the bigger outflow. Later, after 0.5 Myr, we can see fossil outflows, that move comparatively slower than before (at the end of the AGN episode). Velocities reach around $v_{\rm rad} \sim 100$ km s^{-1}. The outflow structures are still similar to the ones analysed before, and expand to around $r \sim 1.2$ kpc.

3.2 Differences in Outflows between Galaxies with AGN and Galaxies with Recently Quiescent AGN

In this part, main outflow parameters such as: mass flow rates (denoted by $\dot{M}$), momentum flow rates (denoted by $\dot{p}$), and energy flow rates (denoted by $\dot{E}$) are analysed. In general, these parameters allow to investigate outflow dynamics. They also can correlate with observed galaxies AGN luminosities. These parameters are calculated by summing over small shells:

$$\dot{M}(r)\Delta r = \sum_{i \in \Delta r} m_i v_{\text{rad},\, i}\ [\mathrm{M}_\odot\ \mathrm{yr}^{-1}], \tag{12}$$

$$\dot{p}(r)\Delta r = \sum_{i \in \Delta r} m_i v^2_{\text{rad},\, i},\ \dot{p} = \dot{M}v\ [\mathrm{L_{Edd}\ c}^{-1}] \tag{13}$$

$$\dot{E}(r)\Delta r = \sum_{i \in \Delta r} \frac{1}{2} m_i v^3_{\text{rad},\, i},\ \dot{E} = \dot{M}v^2/2\ [\mathrm{L_{Edd}}] \tag{14}$$

where M_i represents the mass of the i-th particle and $v_{\text{rad},\, i}$ denotes its radial velocity. Δr is the shell radius which is 50 pc (results do not change significantly from this arbitrary value of Δr). For these calculations particles were filtered with $v_{\rm rad} > 100$ km s^{-1}, which that belong to outflows.

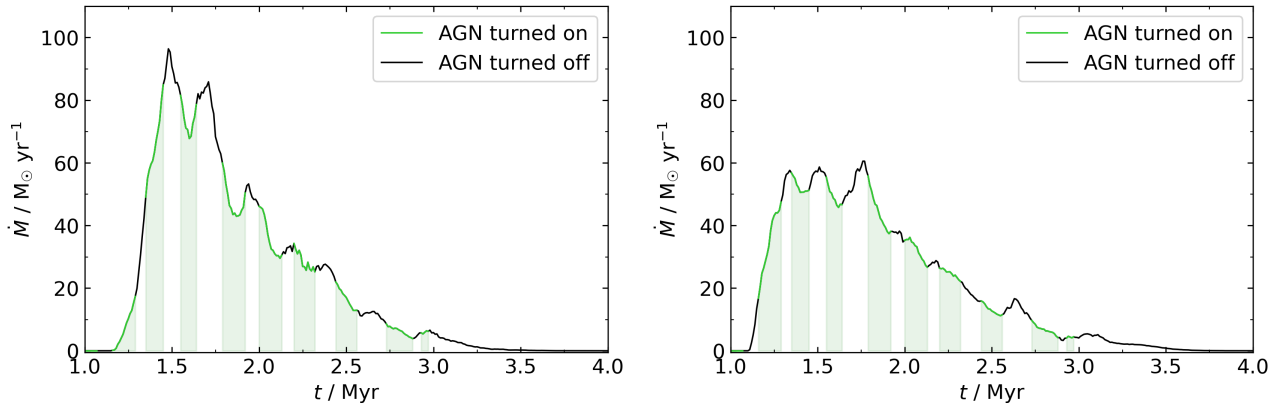

Figure 6. Both diagrams show mass flow rate dependence on time at 0.3 kpc. *Left* the R1A is shown, on the *right* - R1B. Green parts indicate the when the AGN is active, while black means AGN is inactive.

Here, I analyse the differences and similarities between the simulations in terms of main outflow

parameters, when AGN is active and inactive. Figure 6 shows both R1A and R1B simulations mass outflow rates at 0.3 kpc. The curves are inherently different, due to different velocity fields, that were applied, which led to the formation of dissimilar turbulent medium in the first million years of evolution. Therefore, the interaction between the outflows and the rest of medium result in relatively lower $\dot{M}$ values in case of R1B while comparing to R1A. In R1A simulation, the peak value of $\dot{M}$ reaches 97 $M_\odot$ yr^{-1} at $t = 1.5$ Myr, while in R1B it only reaches ~ 60 $M_\odot$ yr^{-1} at three different times $t = 1.3; 1.6; 1.8$ Myr. The average mass flow rate at 0.3 kpc, while AGN is active, in R1A simulation is $\dot{M} = 29$ $M_\odot$ yr^{-1}, which is simmilar to R1B: $\dot{M} = 28$ $M_\odot$ yr^{-1}. However, slightly larger difference is seen if compared when AGN is inactive, for R1A simulation $\dot{M} = 37$ $M_\odot$ yr^{-1} and for R1B $\dot{M} = 30$ $M_\odot$ yr^{-1}.

Even though the values of $\dot{M}$ are different, it is possible to see some similarities. The mass outflow rates peak in both diagrams after the AGN episode, during the inactive phase. This indicates a delay in the outflowing gas, reaching the 0.3 kpc radius, which could be expected. Another common trend that is seen is that the overall $\dot{M}$ values decrease over time, during the whole AGN activity period - from 1 to 3 Myr. One explanation for this could be the fact that since the turbulence isn't driven after the start of the simulation, the gas starts falling to the center quickly, therefore quenching the outflows and thus reducing the mass flow rates, even though the AGN can still be active. Another similarity is that simulations R1A and R1B at 0.6 kpc have respective mass flow rates of 14 and 12 $M_\odot$ yr^{-1} during all the AGN activity phases and 13 and 12 $M_\odot$ yr^{-1} while the AGN is inactive. This is due to the fact that the further the outflows travel, the more quenched they become due to the infalling gas.

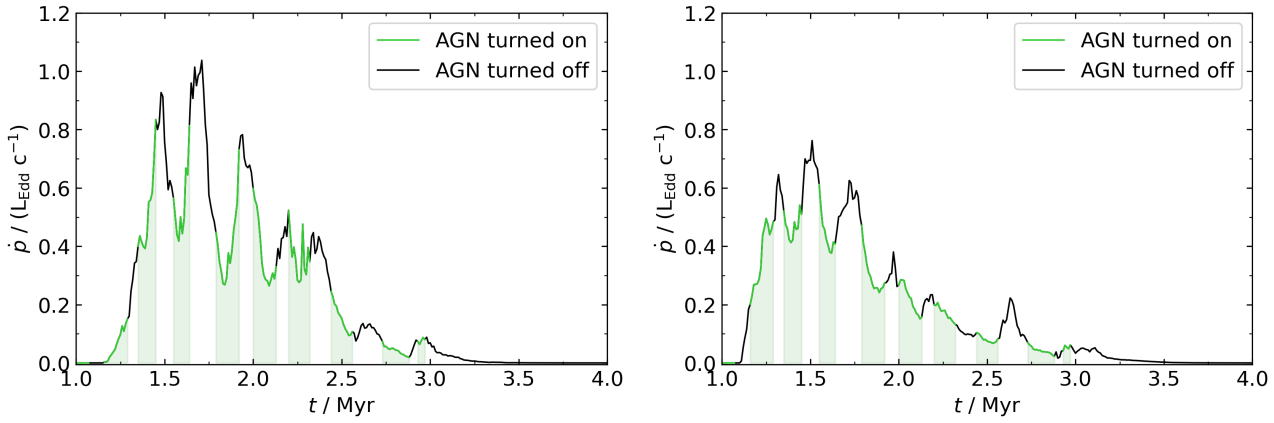

Figure 7. Both diagrams show momentum flow rate dependence on time at 0.3 kpc. *Left* the R1A is shown, on the *right* - R1B. Green parts indicate the when the AGN is active, while black means AGN is inactive.

Figure 7 shows the momentum flow rate dependence on time of R1A and R1B simulations. In the R1A simulation, the first AGN episode, that occurs, does not show any particular feedback effect during the episode and during the first inactivity period. The $\dot{p}$ values are 0 L_{Edd} c^{-1} for the first 1.6×10^5 yr after the start of the first AGN episode. Only after the second AGN episode begins,

it is possible to notice the outflow activity at the 0.3 kpc, which then, further escalates and reaches 0.4 L_{Edd} c^{-1} at the end of the second AGN inactivity phase. The latter pattern is also seen in Figure 6 for the R1A simulation. Referring back to Figure 7, it might seem that the first AGN episode is too short to create outflows for R1A simulation, however it is not the case in R1B simulation. Here, after the first AGN episode, we can notice a rather small delay of several thousand years during the inactivity phase, followed by a rather steep climb of values to 0.2 L_{Edd} c^{-1} at the end of the phase. So the most evident explanation for this difference between the simulations is the dissimilar turbulent medium in which outflows differently interact with it. Momentum flow rates reach peak values of 1.05 and 0.78 L_{Edd} c^{-1} at $t = 1.7;\ 1.55$ Myr for R1A and R1B simulations respectively.

In Figure 8 energy flow rates of the R1A and R1B simulations are shown. While comparing these two diagrams it is possible to see that energetic outflows emerge faster in B velocity field simulation than A (this pattern is seen through out all B group simulations, see Appendix 17). However, in R1A energy flow rates reach around 0.3% L_{Edd} at $t = 1.6$ Myr, and in R1B 0.2% L_{Edd} at $t = 1.3; 1.45$ Myr.

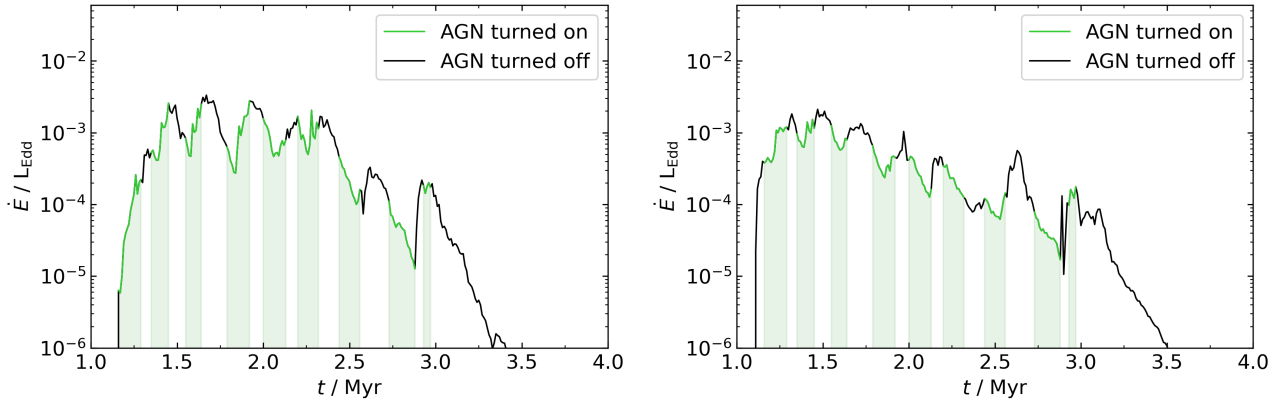

Figure 8. Both diagrams show energy flow rate dependence on time at 0.3 kpc. *Left* the R1A is shown, on the *right* - R1B. Green parts indicate the when the AGN is active, while black means AGN is inactive.

Next, I analyse all of the AGN simulations with multiple episodes with reference to the previously analysed parameters: mass, momentum, and energy flow rates. In Figure 9 the mass flow rates for all of the simulations are seen. I averaged $\dot{M}$ values for episodes when AGN is active and inactive. I choose 0.3 and 0.6 kpc as the radial distances to analyze at, because it is there, where outflows usually peak and start to diminish in terms of mentioned parameters respectively. Also, colored dashed lines that connect the dots do not show any dependence on the sequence of the runs since the AGN luminosity history is generated pseudo-randomly, they are only there to show a particular distance at which the parameter is calculated. On the left A simulation group is shown, and we can see, that for the R1A simulation mass flow rates average ~ 29 $M_\odot$ yr^{-1} while AGN is active, and higher values of ~ 37 $M_\odot$ yr^{-1} are seen when AGN is inactive. Following is R2A simulation, in which averaged mass flow rate values reach ~ 33 and 32 $M_\odot$ yr^{-1} for active and inactive AGN respectively. This is similar to R4A simulation case, however, during the AGN phases on average $\dot{M} \sim 32$ $M_\odot$ yr^{-1} and

33 $M_\odot$ yr^{-1} for inactive phases. The biggest gap is seen in R3A simulation, at which the difference is 13 $M_\odot$ yr^{-1}. When AGN is on, the average mass flow rate values at 0.3 kpc reach $\sim$ 39 $M_\odot$ yr^{-1}. The R5A simulation $\dot{M} \sim$ 34 $M_\odot$ yr^{-1} and 31 $M_\odot$ yr^{-1} for active and inactive AGN. At 0.6 kpc values for all simulations vary around the same value range between 13 and 14 $M_\odot$ yr^{-1} except for R3A, in which the values reach a greater range, that is 15 and 12 $M_\odot$ yr^{-1} for active and inactive AGN phases respectively. In the right panel, we can see a different view and almost a pattern, where $\dot{M}$ values are higher in most of the simulations at 0.3 kpc except for the R1B simulation. However, they are relatively lower when comparing to group A simulations. For R1B simulation, the average mass flow rates are 28 and 30 $M_\odot$ yr^{-1} for AGN active and inactive phases, but for the rest of simulations in B group while AGN is on, the values vary from 30 to 31 $M_\odot$ yr^{-1} and while AGN is off $\dot{M}$ values range from 25 to 26 $M_\odot$ yr^{-1}.

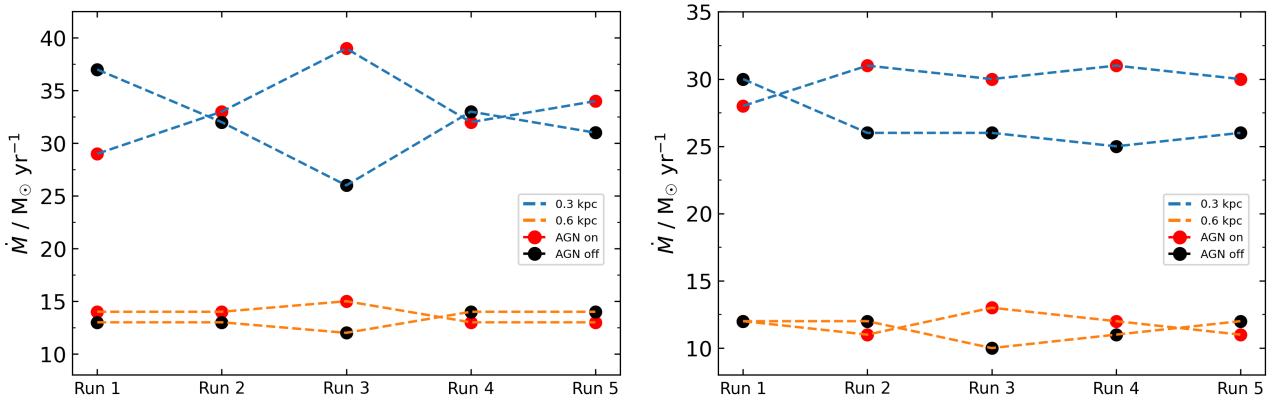

Figure 9. Calculated average mass flow rates for all simulations. Dashed blue line shows values calculated at 0.3 kpc and orange at 0.6 kpc. Red dots show the averages that were calculated while AGN was on and black dots show the averages when AGN was off. On the left are models with A velocity field applied, on the right with B.

For the 0.6 kpc averaged mass flow rate, values vary from 10 to 13 $M_\odot$ yr^{-1}, when the AGN is on and off. In Figure 10 momentum flow rates are averaged and shown in the same manner as in Figure 9. In R1A simulation the momentum flow rate values are 0.26 an 0.4 L_{Edd} c^{-1} when AGN is active and inactive respectively. However, in R2A they are the same 0.32L_{Edd} c^{-1} during both AGN phases. In R3A $\dot{p}$ values differ almost twice - while AGN is on, momentum flow rates reach 0.4 L_{Edd} c^{-1}, and 0.23 L_{Edd} c^{-1} while AGN is off. R4A and R5A share similar values that range from 0.3 to 0.34 L_{Edd} c^{-1} during active and inactive AGN phases. At 0.6 kpc momentum flow rates share similar values, that vary from 0.07 to 0.09 L_{Edd} c^{-1} regardless of the AGN phase. Slightly lower values can be noticed in the right panel regarding the 0.3 kpc distance. R1B $\dot{p}$ values, during AGN activity, are lower than during the inactive phase, and attain only 0.22 L_{Edd} c^{-1}, while other simulations' averaged $\dot{p}$ values range from 0.26 to 0.28 L_{Edd} c^{-1}. Quite the opposite pattern is seen for the values when AGN is off. For values at 0.6 kpc, all runs share the same value range as the A group, except for R3B in which momentum flow rates are 0.1 and 0.06 L_{Edd} c^{-1} when AGN is active and inactive respectively.

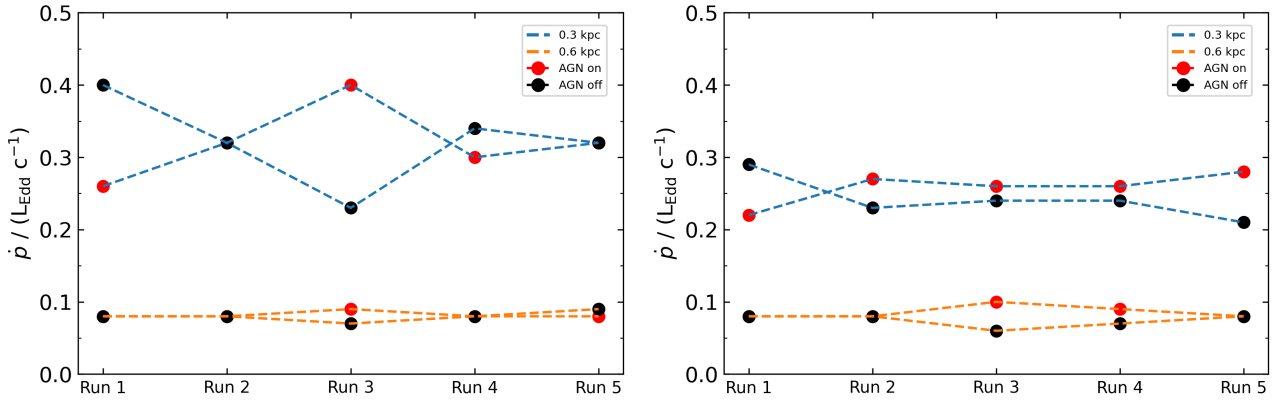

Figure 10. Same as in Figure 9 but instead the $\dot{p}$ is averaged.

For averaged energy flow rates I analyse Figure 11 that was setup in the same manner as Figure 9. In A group at 0.3 kpc, the highest value of $\dot{E}$ reaches $\sim 1 \times 10^{-3}$ $L_{\rm Edd}$ when AGN is active in R3A simulation, and has the lowest value of $\dot{E} \sim 4 \times 10^{-4}$ $L_{\rm Edd}$ when AGN is inactive. Averaged values of energy flow rates in the rest of the simulations when AGN is off are above the ones when AGN is on, but are still similar, in R2A case - almost even. For 0.6 kpc distance, energy flow rates are almost the same, around 1×10^{-4} $L_{\rm Edd}$ and are similar to the ones in the B simulations group. At 0.3 kpc. the values in B group range from 4×10^{-4} to 6×10^{-4} $L_{\rm Edd}$.

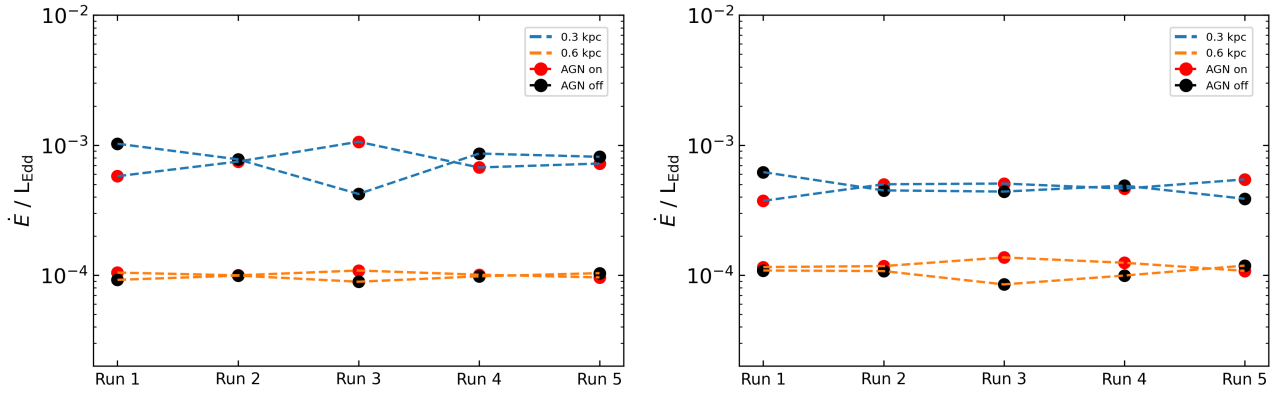

Figure 11. Same as in Figure 9 but instead the $\dot{E}$ is averaged.

3.3 Outflow thermodynamical phases

In this section I will analyse the different gas phases in terms of temperature, that comprise the outflows. Mass outflows are calculated using Equation 12. Gas particles are filtered with $v_{\rm rad} > 100$ km s^{-1} and were sorted by temperature into three intervals: cold ($T < 5 \times 10^4$ K), warm ($5 \times 10^4 < T < 1 \times 10^7$ K), and hot ($T > 1 \times 10^7$ K). This is done to separate atomic and ionised gas. Figure 12 shows just that. These are mass flow rate diagrams during three different times ($t = 1.5; 1.55; 1.6$ Myr) that depict a transition from inactive AGN phase to active in R1A simulation. In the left panel we see that overall the mass flow rates reach around $\dot{M} = 90$ M$_\odot$ yr^{-1} around $r \sim 0.3$ kpc., however,

the cold gas phase transfer largest amount of gas compared with other phases. That is to be expected, since the AGN is not currently active. The hot phase is significant and mass flow rates reach $\dot{M} = 30\ \mathrm{M}_\odot\ \mathrm{yr}^{-1}$ at $r = 0.2$ kpc. An insignificant amount of warm gas transfer only a few $\mathrm{M}_\odot\ \mathrm{yr}^{-1}$. When AGN turns on (middle panel) we can see the decrease of $\dot{M}$ values of cold outflows, and increase in warm component. The gas is heated by the AGN activity. We can also see the increase of mass flow rate in the $r < 0.1$ kpc region. Here, gas particles are accelerated by the energetic AGN winds and are hotter than $T > 1 \times 10^7$ K. They comprise all of the $\dot{M}$ values in this region. This effect is more prominent on the right panel at $t = 1.6$ Myr, while AGN activity is still ongoing. At $r = 0.1$ kpc mass flow rates are $\dot{M} = 38\ \mathrm{M}_\odot\ \mathrm{yr}^{-1}$ for the hot outflows, and past this radial coordinate values start to diminish until 0.6 kpc. Cold gases transfer similar amount of mass at $r = 0.3$ kpc. For the warm gases, their mass flow rates reach $\dot{M} = 25\ \mathrm{M}_\odot\ \mathrm{yr}^{-1}$ at $r = 0.4$ kpc. All outflow mass flow rates peak at $\sim 70\ \mathrm{M}_\odot\ \mathrm{yr}^{-1}$ ($r = 0.35$ kpc). Overall, for this particular simulation the mass flow rates seem to diminish after the fourth AGN episode starts.

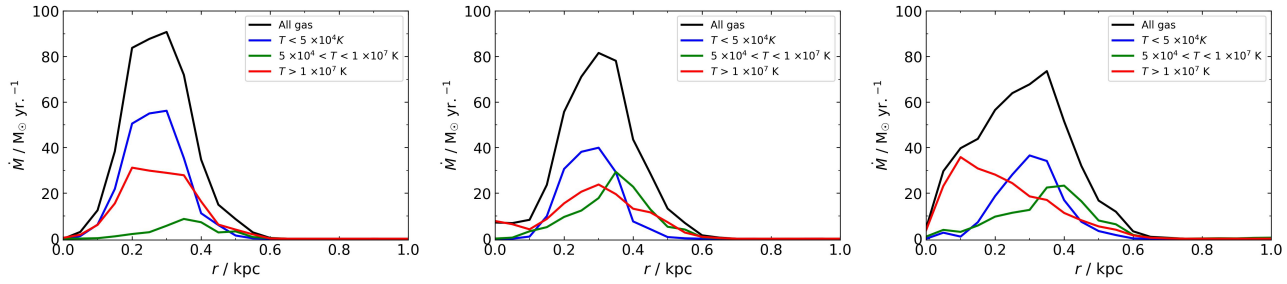

Figure 12. Mass flow rate dependency on distance (in kpc) in R1A simulation during $t = 1.5$, 1.55 and 1.6 Myr in the left, middle, and right panels respectively. Mass flow rates are divided into different temperature intervals: all gas (black), $T < 5 \times 10^4$ K (blue), $5 \times 10^4 < T < 1 \times 10^7$ K (green), $T > 1 \times 10^7$ K (red).

In the following Figure 13 same temperature divided mass flow rate diagrams are shown. Mass flow rates are overall larger due to continuous AGN episode, that lasts for 1 Myr. In the left diagram, at $r = 0.5$ kpc values of mass flow rates peak at $\sim 150\ \mathrm{M}_\odot\ \mathrm{yr}^{-1}$. However, most cold outflows do dominate, since at the same distance, $\dot{M} \sim 88\ \mathrm{M}_\odot\ \mathrm{yr}^{-1}$. Lower values of $\sim 54\ \mathrm{M}_\odot\ \mathrm{yr}^{-1}$ are due to hot outflows still transferring mass from the center, while AGN is still active at this time. 200 kyr after the AGN becomes inactive, the hot outflowing gas are effectively cooled by surrounding infalling gas and the small peak in the $r < 0.25$ kpc region is the comprised only of cold fossil outflows transferring mass at a rate of $23\ \mathrm{M}_\odot\ \mathrm{yr}^{-1}$. Overall, fossil outflows start to diminish in terms of mass flow rate and peak at $\sim 125\ \mathrm{M}_\odot\ \mathrm{yr}^{-1}$, while cold outflows reach $\sim 90\ \mathrm{M}_\odot\ \mathrm{yr}^{-1}$. The hot outflow phase is diminished and reaches only $25\ \mathrm{M}_\odot\ \mathrm{yr}^{-1}$, while warm component attains $\dot{M} = 88\ \mathrm{M}_\odot\ \mathrm{yr}^{-1}$. In the right panel, at $t = 2.5$ Myr hot and warm outflows are diminished, but the cold outflows are still prominent and $\dot{M}$ reaches values of $\sim 50\ \mathrm{M}_\odot\ \mathrm{yr}^{-1}$ in the range of $r = 0.5 - 0.7$ kpc. The outflows lose momentum due to collisions with regions of cold infalling gas, thus effectively cooling them and reducing their capabilities to transfer more mass out of the bulge medium.

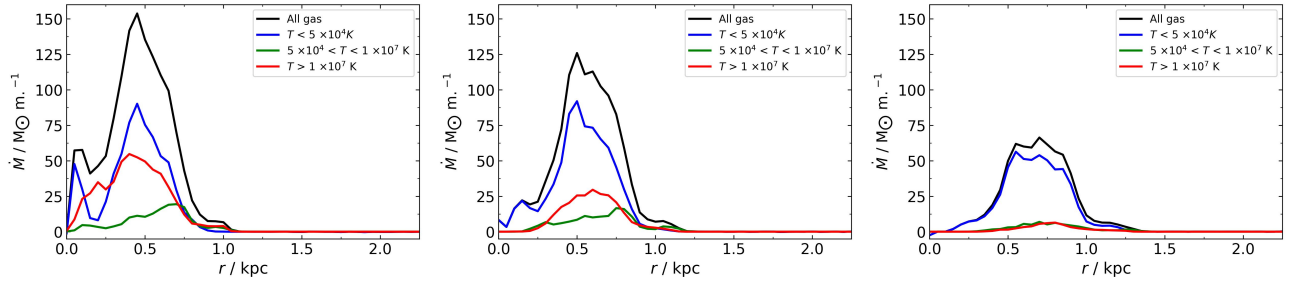

Figure 13. Mass flow rate dependency on distance (in kpc) in CA simulation during $t = 2$, 2.2 and 2.5 Myr in the left, middle, and right panels respectively. Mass flow rates are divided into different temperature intervals: all gas (black), $T < 5 \times 10^4$ K (blue), $5 \times 10^4 < T < 1 \times 10^7$ K (green), $T > 1 \times 10^7$ K (red).

3.4 Outflowing mass

The following analysis will be about the amount of gas, that is pushed with outflows in various simulations. In Figure 14 the left and middle panels a winding pattern of the curves is seen, due to the multiple AGN activity episodes. However, in continuous simulation the curve is comparatively smooth. That is to be expected, since the outflows are always driven during the AGN episode, therefore they carry more mass than those created by an intermittent AGN episode. The amount of gas mass that is being pushed from the R1A simulation center with outflows moving with speeds $v_{\rm rad} > \sigma$ at $t = 2$ Myr is $\sim 5 \times 10^7 {\rm M}_\odot$. At this time average temperatures of these outflows reach $T_{\rm avg} \simeq 10^{6.8}$ K. These outflows dissipate at around $t = 4$ Myr. Quite a significant portion of these outflows are fast and blue line in R1A simulation depicts that. Amount of mass moving with fast outflows fluctuates from 1.5 to $2 \times 10^7 {\rm M}_\odot$ from $t = 1$ Myr to $t = 2.5$ Myr. Green line separates the hottest and most energetic outflowing gases. Since the hot gases are diffuse, the do not transfer that much mass, so overall values are relatively low and reach around $M = 1 \times 10^7 {\rm M}_\odot$ at $t = 2$ Myr and comprise only 20% of all outflowing gas (red line) at that particular time. In R3A simulation, the M values are lower, the red line peaks $M = 4 \times 10^7 {\rm M}_\odot$ at $t = 1.75$ Myr. That could be because of the specific R3 AGN luminosity history pattern, since in Figure 15, R3B simulation (middle panel), the outflowing mass is very similar around the same time $t = 1.75$ Myr. Ratio, however, between green and red line is higer in R3A simulation, than in R3B. Green line comprises 26% of the red line, while in R3B its 22%.

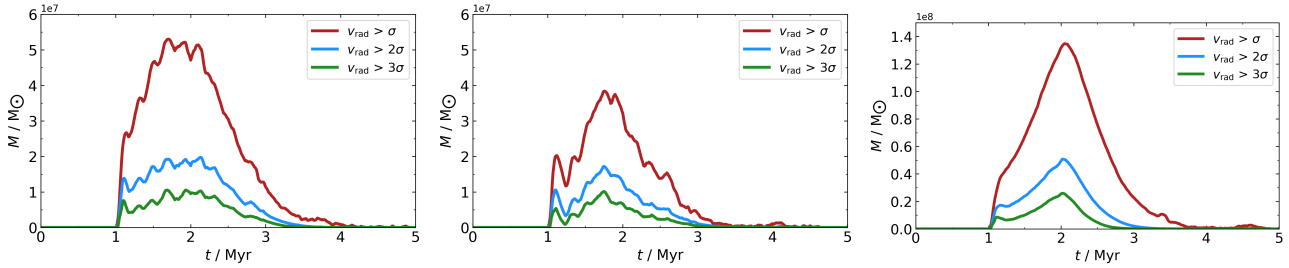

Figure 14. Outflowing mass $M(\mathrm{M}_\odot)$ dependence on time in R1A (*left*), R3A (*middle*), and CA (*right*) simulations. Lines show different thresholds of velocity, by which gas are filtered and summed afterwards through the whole simulation time.

In all of the simulations, except continuous ones, outflows diminish at around $t = 4$ Myr. On the left panel (see Figure 15) in R1B simulation, outflowing mass with radial velocities greater than σ reach $M = 5.5 \times 10^7 \mathrm{M}_\odot$. Around the same time at $t = 1.75$ Myr both blue and green lines peak at ~ 2.25 and $\sim 1.25 \mathrm{M}_\odot$. The average temperature for the gas that is moving with $v_{\mathrm{rad}} > 3\sigma$ is $T_{\mathrm{avg}} \simeq 10^{7.2}$ K. Green component comprises 21% of the red one. After the AGN episodes end at $t = 3$ Myr, average temperatures for the same outflows remain the same, and for all outflowing gas with velocities $v_{\mathrm{rad}} > \sigma$, $T_{\mathrm{avg}} \simeq 10^{6.3}$ K.

For the continuous simulations, the amount of outflowing mass in CA simulation with velocities greater than σ peak at $t = 2$ Myr, just at the same time AGN turns off. Outflowing mass is $M = 1.3 \times 10^8 \mathrm{M}_\odot$. Average temperature of these gases is $T_{\mathrm{avg}} \simeq 10^{7.2}$ K. For the outflows with $v_{\mathrm{rad}} > 3 \times \sigma$, total outflowing mass is $M = 2.5 \times 10^7 \mathrm{M}_\odot$ and the average temperature is $T_{\mathrm{avg}} \simeq 10^{7.8}$ K. Relatively, this green component comprises around 19% of the red one. Outflows also fade at around $t = 4$ Myr. Next in CB simulation, peak outflowing mass is $M = 1.3 \times 10^8 \mathrm{M}_\odot$, however compared to CA simulation, for the outflowing mass the values are slightly greater and reach $M = 3.1 \times 10^7 \mathrm{M}_\odot$. Though, the average temperature is lower - $T_{\mathrm{avg}} \simeq 10^{7.6}$ K and comprises 23%.

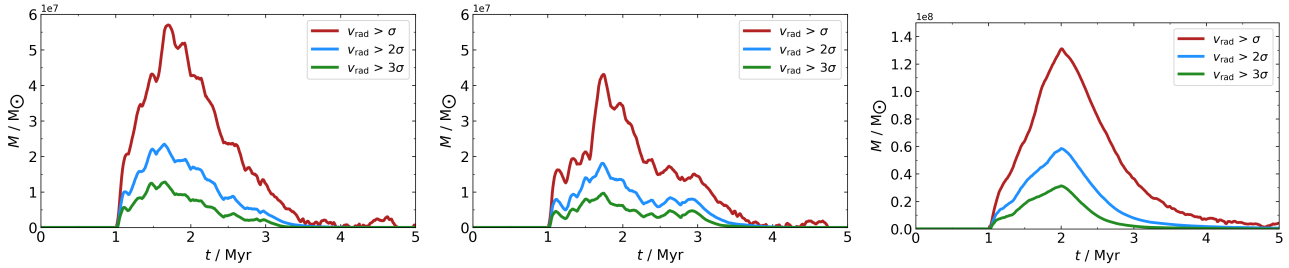

Figure 15. Outflowing mass $M(\mathrm{M}_\odot)$ dependence on time in R1B (*left*), R3B (*middle*), and CB (*right*) simulations. Lines show different thresholds of velocity, by which gas are filtered and summed afterwards through the whole simulation time.

4 Discussion

Outflows take shapes of elongated cones before transforming into uneven bubbles. The aftermath of these flowing bubbles colliding with infalling gas is the suppression outflows and reduction of their radial velocity. Hot ouflows are the most energetic near the center at $r < 0.3$ kpc and tend to follow the path of the least resistance in the turbulent medium, condensing surrounding gas into clumps.

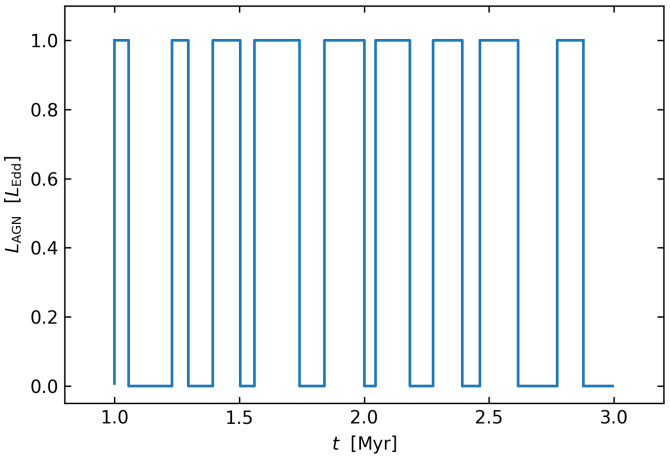

Figure 16. R3 AGN luminosity history. Blue line, square wave like pattern shows AGN activity over 2 Myr. The total activity time is 1 Myr, thus achieving the duty cycle of $\delta_{\text{duty}} = 0.5$.

Only a slight variation in overall values is seen due to stochastic turbulent field in the bulge medium. Though, in group B simulations, outflows are able to escape the center faster than the group A. However, more distinct patterns in outflow parameter results come from the pseudo-random AGN luminosity histories. For example, outflowing mass distribution in timeframe of 2 Myr in R3 simulations (both A and B groups) have very similar patterns and have relatively lower values than R1 simulations. However, we can notice in Figure 16 that the longer (periodic) AGN episodes are clustered more in the middle of the whole AGN episode as oppose to the R1 AGN luminosity distribution (see Figure 1), which is more uniform. Turbulent medium forms 1 Myr after the simulations start, but after that, the turbulence is not driven, and gas fall into the center because of gravitational potential, that was also applied to the simulations. That means, while the simulations evolve, turbulent medium becomes less evident, and later on it becomes more difficult for outflows to move away in such medium. That is why in R3 case, total outflowing mass is lower than in those simulations, that have longer AGN episodes in the beginning; gas fall into the center and dense gases start circulating the AGN, thus meaning more energy for outflows to push through these cold, dense gases is needed. If the periodic AGN episodes are not long enough at the start of the whole AGN episode, it is harder for outflows to escape in the long run, since the inner 100 pc might not have that many diffuse channels for outflows to travel through. For the same reason, we see peaks of outflowing mass earlier in R1 simulations, rather than later in R3 ones.

Fossil outflows are effectively cooled and consist mostly of cold gas. They should be detectable between the episodes, and in some instances (R1A simulation) average mass flow rate values of fossil outflows exceed the ones, of normal AGN episode driven outflows. One explanation for this could simply be the delay, for outflows to propagate to certain distance, where I measure the properties. However when the whole AGN episode ends, fossil outflows are not noticeable - they are effectively stopped by infalling gas. However, if AGN episode is continuous and lasts for 1 Myr, fossil outflows can be detected for more than 2 Myr (see Figure 15 right panel) which fit into analytical expectations, that outflows may last up to 10 times the duration of the AGN episode (King et al., 2011).

Conclusion

In this thesis 14 idealised hydrodynamical simulations were analysed, in which outflow evolution was tracked during AGN episodes and after.

Models were grouped into A and B groups due to different stochastic turbulent velocity fields applied to them. Each group comprised of 7 simulations: 1 control (without AGN), 1 continuous (AGN is active for 1 Myr), and 5 simulations, with different AGN histories (lasting 2 Myr, with $f_{\rm duty} = 0.5$), which were the main focus of this work. Main conditions were that $M_{\rm BH} = 10^8 {\rm M}_\odot$, $L_{\rm AGN} = L_{Edd}$, and that the gas were placed in a spherically symmetrical sphere, with a radius of $R_{\rm out} = 2.57$ kpc. More detailed initial conditions are described in Table 2. After qualitatively and quantitatively analysing the outflow parameters and their dependence on time and distance, main results are the following:

1. In group A simulations, the outflows are not as prominent compared to CA simulation in terms of size and distance they travel from the center. In R4A simulation outflows fade more quickly, though they can reach radial velocities of $v_{\rm rad} > 300$ km s^{-1} (see Figure 4). They reach distances of around $r = 0.6$ kpc before they begin to fade. However, they are more concentrated near the center at $r < 0.3$ kpc. Continuous AGN models have larger and more massive outflows reaching around $r \sim 1.2$ kpc before begining to fade.

2. In R1A simulation mass flow rates peak values are $\dot{M} = 97$ M$_\odot$ yr^{-1} at $r = 0.3$ kpc, while $t = 1.5$ Myr. Other simulations show lower peak values of mass flow rates, but in general, their momentum and energy rates are similar. Next, the average mass outflow rates were calculated for all of the AGN episodes and periods of quiescent AGN. In some simulations, when AGN is off, mass flow rates on average can be higher that the ones with AGN on, in others it can be the opposite. At 0.3 kpc averaged mass flow rates vary relatively more than at 0.6 kpc, however they are greater and reach up to ~ 39 M$_\odot$ yr^{-1}.

3. I separated the mass flow rates into cold, warm, and hot gas components, when analysing the radial mass flow rate dependency: the outflows during AGN inactivity phase (R1A simulation) are mostly comprised of cold ($T < 5 \times 10^4$ K) gas component, but hot ($T > 10^7$ K) outflows are still prevalent and reach $\dot{M} = 30$ M$_\odot$ yr^{-1} at $r = 0.2$ kpc. After 100 kyr mostly hot gas transfer the mass from the center, while maintaining $\dot{M} = 38$ M$_\odot$ yr^{-1}. Regarding the outflowing mass, R1A and R1B peak outflowing mass values are greater than of R3A and R3B, which means the AGN luminosity history distribution can affect the cumulative outflowing mass at particular times. Fast moving outflows ($v_{\rm rad} > 3 \times \sigma$) are hot and reach the average temperatures of $T_{\rm avg} \simeq 10^{7.2}$ K. They also comprise from 19% to 26% of generally filtered outflowing mass ($v_{\rm rad} > \sigma$). Continuous AGN simulations have peak outflowing mass of $M = 1.3 \times 10^8 {\rm M}_\odot$ with ($v_{\rm rad} > \sigma$).

References

Bîrzan L., Rafferty D., Nulsen P., McNamara B., Röttgering H., Wise M., Mittal R., 2012, Monthly Notices of the Royal Astronomical Society, 427, 3468

Cicone C., et al., 2014, Astronomy & Astrophysics, 562, A21

Dalrymple R. A., 2007, Department of Civil Engineering, Baltimore, p. 32

Dehnen W., Aly H., 2012, Monthly Notices of the Royal Astronomical Society, 425, 1068

Dobbs C., Pringle J., 2013, Monthly Notices of the Royal Astronomical Society, 432, 653

Dubinski J., Narayan R., Phillips T., 1995, arXiv preprint astro-ph/9501032

Ferrarese L., Merritt D., 2000, ApJL, 539, L9

Fluetsch A., et al., 2019, Monthly Notices of the Royal Astronomical Society, 483, 4586

Guo H., Li C., Zheng Z., Mo H., Jing Y., Zu Y., Lim S., Xu H., 2017, The Astrophysical Journal, 846, 61

Häring N., Rix H.-W., 2004, ApJL, 604, L89

Hobbs G., Lorimer D., Lyne A., Kramer M., 2005, Monthly Notices of the Royal Astronomical Society, 360, 974

Hopkins P. F., Hernquist L., Martini P., Cox T. J., Robertson B., Di Matteo T., Springel V., 2005, The Astrophysical Journal, 625, L71

Ishibashi W., Fabian A., 2018, Monthly Notices of the Royal Astronomical Society, 481, 4522

King A., Zubovas K., Power C., 2011, Monthly Notices of the Royal Astronomical Society: Letters, 415, L6

Kormendy J., Ho L. C., 2013, Annual Review of Astronomy and Astrophysics, 51, 511

Malkin Z., 2019, The Astronomical Journal, 158, 158

Marasco A., et al., 2020, Astronomy & Astrophysics, 644, A15

Mashchenko S., Wadsley J., Couchman H. M. P., 2008, Science, 319, 174

Maskeliūnas 2022, Vilniaus Universitetas

McConnell N. J., Ma C.-P., 2013, The Astrophysical Journal, 764, 184

Price D. J., Federrath C., 2010, Monthly Notices of the Royal Astronomical Society, 406, 1659

Read J., Hayfield T., 2012, Monthly Notices of the Royal Astronomical Society, 422, 3037

Sazonov S. Y., Ostriker J. P., Ciotti L., Sunyaev R. A., 2005, MNRAS, 358, 168

Schawinski K., Koss M., Berney S., Sartori L. F., 2015, Monthly Notices of the Royal Astronomical Society, 451, 2517

Smethurst R., Simmons B., Lintott C., Shanahan J., 2019, Monthly Notices of the Royal Astronomical Society, 489, 4016

Springel V., 2005, Monthly notices of the royal astronomical society, 364, 1105

Springel V., et al., 2005, nature, 435, 629

Stuber S. K., et al., 2021, Astronomy & Astrophysics, 653, A172

Tartėnas M., Zubovas K., In preparation, Monthly Notices of the Royal Astronomical Society

Wendland H., 1995, Advances in computational Mathematics, 4, 389

Zubovas K., King A., 2012, The Astrophysical Journal Letters, 745, L34

Zubovas K., King A. R., 2019, General Relativity and Gravitation, 51, 1

Zubovas K., Bialopetravičius J., Kazlauskaitė M., 2022, Monthly Notices of the Royal Astronomical Society, 515, 1705

Gediminas Maskeliūnas

FOSILINIŲ GALAKTINIŲ TĖKMIŲ TYRIMAS

Santrauka

Galaktikose esančios supermasyvių juodųjų skylių masės koreliuoja su galaktikų charkteringais parametrais. Tėkmės - vienas iš būdų paaiškinti $M_{\mathrm{SMBH}} - \sigma$ ir kitus panašius sąryšius. Tėkmės, taip pat yra viena iš grįžtamojo ryšio formų į galaktiką ir atsiranda aktyviam galaktikos branduoliui kuriant vėją. AGN vėjas stumia dujas, kurios keliauja tolyn nuo galaktikos centro ir gali būti stebimos. Taip pat, tėkmės yra išskiriamos ir į fosilinės tėkmes, kuomet AGN šviesis ir tėkmių parametrai glaudžiai nekoreliuoja. Šiame darbe buvo leidžiami hidrodinaminiai modeliai skirtingomis pseudoatsitiktinai sugeneruotomis AGN šviesio istorijomis. Jie buvo lyginami su mažiau realistiškais modeliais, kuriuose AGN veikė 1 mln. m. Šio darbo tiklas yra ištirti galaktinių tėkmių evoliuciją esant daugeliui AGN epizodų, išvados yra šios:

1. Modeliuose su keliais AGN epizodais, tėkmės nėra tokios ryškios savo dydžiu bei atstumu, kurį gali nukeliauti nuo centro, palyginus su pastovaus AGN šviesio modeliu. Modelyje, su keliais AGN epizodais, nors ir tėkmės nuslopsta greičiau, jos gali pasiekti greičius $v_{\mathrm{rad}} > 300$ km s^{-1} (žr 4 pav.). Tėkmės siekia iki $r = 0.6$ kpc prieš pradedant nykti. Kita vertus, jos yra labiau koncentruotos ties $r < 0.3$ kpc. Pastovaus šviesio AGN modeliai pasižymi didesnėm ir masyvesnėm tėkmėm, kurios siekia $r \sim 1.2$ kpc prieš pradedant slopti.

2. Modelyje su keliais AGN epizodais masės pernašos spartos didžiausios vertės siekia $\dot{M} = 97$ M$_\odot$ yr^{-1} ties $r = 0.3$ kpc, $t = 1.5$ mln. m. laiku. Kitų modelių didžiausios $\dot{M}$ vertės buvo mažesnės, tačiau bendru atveju, jų judesio kiekio bei energijos pernašos spartos buvo panašios. Toliau, visiems modeliams su keletu AGN epizodų buvo suskaičiuotos vidutinės masės pernašos spartos kuomet AGN buvo aktyvus ir neaktyvus. Dviejuose modeliuose, kuomet AGN epizodas nevyko, masės pernašos spartos vertės vidutiniškai buvo didesnės nei esant AGN epizodams, kituose modeliuose - atvirkščiai. Atstumu $r = 0.3$ kpc vidutinės $\dot{M}$ vertės buvo reliatyviai didesnės nei tos, suskaičiuotos ties $r = 0.6$ kpc ir siekė iki $\sim$ 39 M$_\odot$ yr^{-1}.

3. Analizuojant, buvo atskirtos masės pernašos spartos komponentės pagal temperatūrą: šaltos, šiltos bei karštos. Modelyje, su keletu AGN epizodų, tėkmių $\dot{M}$ vertės daugiausia sudarytos iš šaltos dujų dujų komponentės ($T < 5 \times 10^4$ K), tačiau karštos ($T > 10^7$ K) tėkmės yra reikšmingos ir siekia $\dot{M} =$ 30 M$_\odot$ yr^{-1} ties $r = 0.2$ kpc ($t = 1.5$ mln. m.). Po 100 tūkst. m. AGN epizodui prasidėjus, daugiausia karštos tėkmės perneša medžiagą šalia centro, masės pernašos sparta siekia $\dot{M} = 38$ M$_\odot$ yr^{-1}. Greitai judančios tėkmės ($v_{\mathrm{rad}} > 3 \times \sigma$) modeliuose su keliais AGN epizodais yra karštos ir jų vidutinė temperatūra siekia $T_{\mathrm{avg}} \simeq 10^{7.2}$. Taip pat šios greitos tėkmės gali sudaryti nuo 19% iki 26% visų masę pernešančių tėkmių ($v_{\mathrm{rad}} > \sigma$). Pastovaus AGN epizodo modeliai pasižymi masės, pernešamos tėkmėmis ($v_{\mathrm{rad}} > \sigma$), vertėmis $M = 1.3 \times 10^8$M$_\odot$.

Pagrindinės sąvokos: aktyvūs galaktikos branduoliai, AGN, tėkmės, turbulentiškos dujos, SPH.

Gediminas Maskeliūnas

INVESTIGATING FOSSIL GALACTIC OUTFLOWS

Summary

The masses of supermassive black holes in galaxies correlate with the galaxies' characteristic parameters. Outflows are one way to explain $M_{\mathrm{SMBH}} - \sigma$ and other similar correlations. Outflows are a form of feedback and are produced by the active galactic nucleus (AGN) creating winds. The AGN wind pushes gas that travels away from the centre of the galaxy and can be observed. Some outflows are peculiar in that the AGN luminosity and outflow parameters are uncorrelated. These outflows can be called fossil, due to the fact that by the time they are observed, the AGN has become inactive. In this work I run hydrodynamical simulations of AGN feedback on idealised turbulent gas shells, with multiple uniformly generated AGN episodes, and compare them to less realistic ones where AGN episode is continuous for 1 Myr. The aim of this thesis is to investigate the evolution of galactic outflows with multiple AGN episodes. The conclusions are the following:

1. In simulations, with multiple AGN episodes, the outflows are not as prominent compared to continuous AGN episode simulation in terms of size and distance they travel from the center. In one of the simulation with multiple AGN episodes outflows fade rather quickly, though they can reach radial velocities of $v_{\mathrm{rad}} > 300$ km s^{-1} (see Figure 4). They reach distances of around $r = 0.6$ kpc before they begin to fade. However, they are more concentrated near the center at $r < 0.3$ kpc. Continuous AGN simulations have larger and more massive outflows reaching around $r \sim 1.2$ kpc before begining to fade.

2. In a simulation with multiple AGN episodes, mass flow rates peak values are $\dot{M} = 97$ M$_\odot$ yr^{-1} at $r = 0.3$ kpc, while $t = 1.5$ Myr. Other simulations show lower peak values of mass flow rates, but in general, their momentum and energy rates are similar. Next, the average mass outflow rates were calculated for all of the AGN episodes and periods of quiescent AGN. In some simulations, when the AGN is off, mass flow rates on average can be higher that the ones with AGN on, in others it can be the opposite. At 0.3 kpc averaged mass flow rates vary relatively more than at 0.6 kpc, however they are greater and reach up to ~ 39 M$_\odot$ yr^{-1}.

3. I separated the mass flow rates into cold, warm, and hot gas components, when analysing the radial mass flow rate dependency: the outflows during AGN inactivity phase (multiple AGN episodes simulation) are mostly comprised of cold ($T < 5 \times 10^4$ K) gas component, but hot ($T > 10^7$ K) outflows are still prevalent and reach $\dot{M} = 30$ M$_\odot$ yr^{-1} at $r = 0.2$ kpc. After 100 kyr mostly hot gas transfer the mass from the center, while maintaining $\dot{M} = 38$ M$_\odot$ yr^{-1}. Regarding the outflowing mass (in simulations with multiple AGN episodes) fast moving outflows ($v_{\mathrm{rad}} > 3 \times \sigma$) are hot and reach the average temperatures of $T_{\mathrm{avg}} \simeq 10^{7.2}$ K. They also comprise from 19% to 26% of generally filtered outflowing mass ($v_{\mathrm{rad}} > \sigma$). Continuous AGN simulations have peak outflowing mass of $M = 1.3 \times 10^8$M$_\odot$ with ($v_{\mathrm{rad}} > \sigma$).

Keywords: active galactic nuclei, AGN, outflows, turbulent gas, SPH.

Appendix

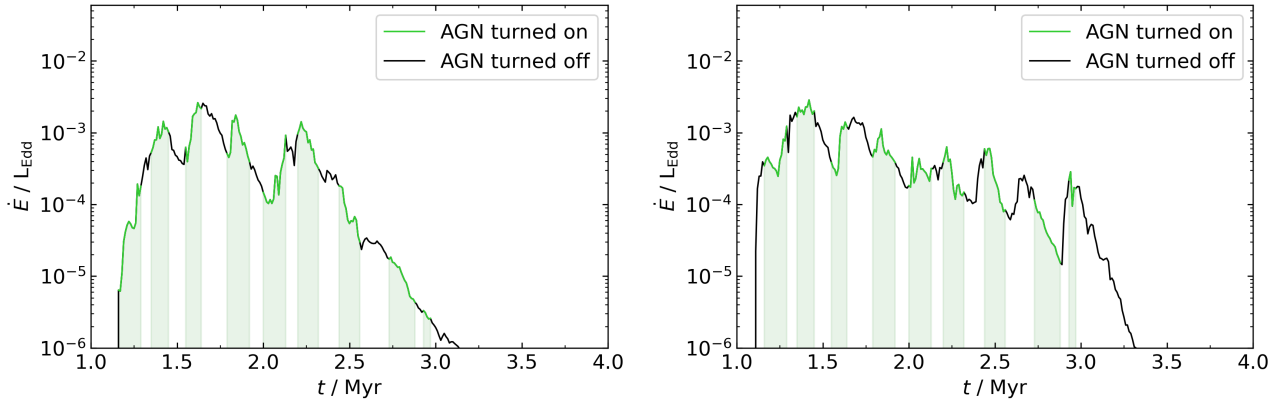

Figure 17. Both diagrams show energy flow rate dependence on time at 0.3 kpc. *Left* the R2A is shown, on the *right* - R2B. Green parts indicate the when the AGN is active, while black means AGN is inactive. R2B outflows emerge more quickly than R2A.